

# Microstructural Evolution and Damage Mechanisms in Pb-Free Solder Joints During Extended $-40^{\circ}\text{C}$ to $125^{\circ}\text{C}$ Thermal Cycles

Steven O. Dunford  
Nokia Mobile Phones,  
Irving, TX

Anthony Primavera, Ph.D. and  
Michael Meilunas  
Universal Instruments Corporation  
Binghamton, NY

## Abstract

A comparative study of package-to-board interconnections of a 1.27mm pitch BGA package using two Pb-free alloys and Sn-Pb solder in extended  $-40$  to  $125^{\circ}\text{C}$  thermal cycling is described. The microstructural evolution, intermetallic compound growth, and progressive damage in the solder joints were documented using visual, x-ray, SEM, and EDS analysis.

The analyses indicate that intermetallic compound growth in the Pb-free solder joints can contribute to void retention in Pb-free solders. Sn/Ag intermetallic plates often formed across the grain boundaries and redirected or retarded crack propagation in many instances. In addition, Sn-whiskers were found inside voids and intermetallic formations extending outward from Sn/Ag and Sn/Ag/Cu solder joints as the number of temperature cycles increased. Crack propagation included the formation of vertical and horizontal cracks in random solder joints. The preferred propagation path of the vertical cracks is shown to be through the large angle grain boundaries in the solder. Spalling or separation of portions of the solder joints can also occur.

The observations provide insight into the effects of long-term thermal mechanical stresses and the attendant failure mechanisms in Pb-free solder interconnections.

**Key Words:** *Solder, lead-free, Sn whisker, intermetallic compounds, grain boundary, BGA, reliability, OSP, ENIG, spalling.*

## Introduction

A number of studies have been reported to determine the properties of Pb-free solders.<sup>1-5</sup> A study of the alloys alone does not consider the variations in solder joint metallurgy and interfacial reactions introduced from the PWB surface finish<sup>6</sup> and component termination. The properties and thickness of the intermetallic compounds formed at the solder interfaces directly affects the reliability of solder joints.<sup>6</sup> Differences in crack propagation have been reported but not sufficiently evaluated. Therefore, this study was undertaken to evaluate the reliability, microstructure, and damage mechanisms of Pb-free solder joints on organic solder preservative (OSP) and electroless nickel-immersion gold (ENIG) surface finishes.

Solder joints were formed using Sn3.5Ag and Sn3.8Ag0.7Cu Pb-free solders and control samples using Sn37Pb solder balls and Sn62 solder paste. Components were custom-made 1.27mm pitch daisy chained BGAs with Cu pads and an ENIG surface finish. Bonding a glass slide to the BGA substrate simulated the presence of a silicon die.

Soldered assemblies were tested for electrical continuity, visually inspected, and evaluated for voiding using x-ray. Assemblies were then thermally cycled from  $-40^{\circ}\text{C}$  to

$125^{\circ}\text{C}$ . Continuity of the daisy chain was continuously monitored with a 300-ohm trigger indicating a failure. As events were detected, failed samples as well as good samples were removed for evaluation. X-ray and cross sectional analysis using SEM and EDS were used to evaluate samples and to document metallurgical changes, and failure mechanisms in the solder joints.

This paper will compare the structure and location of the intermetallic formations and the differences in reliability performance for each assembly configuration. It will show evidence that Sn/Ag intermetallic plates can redirect or retard crack growth when they form across large angle grain boundaries. Some potential risks associated with high Sn solders are identified by the presence of Sn whiskers inside voids and Sn rich protrusions on the outside of some Pb-free solder joints. Spalling of solder from the joint due to vertical and horizontal

crack propagation along large angle grain boundaries in the solder joints, is identified as an additional reliability exposure. Board level reliability results are discussed in a companion paper.<sup>8</sup>

## Experimental

A total of 158 components were assembled with eight BGAs to each PWB. The Solder balls on the components

were Sn3.5Ag (SnAg), Sn3.8Ag0.7Cu (SAC), and Sn37Pb (SnPb). The solder paste used to attach the components matched the solder ball alloy with the exception of the SnPb where Sn62 was used for attachment. Sixty-four components were assembled using SnAg, sixty-two using SAC solder paste, and thirty-two components were assembled using Sn62 solder paste. One half of each set were assembled on copper/OSP finished PWBs and the other half were assembled on electroless nickel immersion gold (ENIG) finished PWBs. One sample of each surface finish and solder combination was taken after assembly to establish baseline conditions. PWBs were 1.52mm thick multilayered panels of tetrafunctional FR-4 with a glass transition temperature of 175°C.

### Reflow Profile Optimization

An optimum reflow profile was developed for each solder alloy using a misaligned screen print. The stencil alignment and solder print were 70% offset in one axis from the solder pads and run through the reflow oven. Both ramp and soak and ramp-to-spike oven profiles were evaluated. Profiles yielding the highest wetting or spreading on the solder pad and lowest void content determined optimal profiles for each solder alloy. All profile development was conducted on ENIG surface finished PWBs.

A forced air convection reflow soldering systems consisting of 3 top and bottom heating zones and one cooling zone was used. The 3-zone oven essentially presents a non-optimal reflow situation but the results proved satisfactory. Three K-type thermocouples were attached to the test board and 2 were placed on the underside components attached to the board Ramp and soak style profiles provided the best wetting and lowest voiding with this equipment. All reflow was conducted in ambient atmospheric conditions. The measured times and temperature ranges for the Pb-free solders are shown in Table 1.

**Table 1 - Reflow Profile - Measured Parameter Ranges for Pb-Free Solder**

| TC              | Max. rising Slope °C/s | Rise time 30-150°C | Soak Time 150-170°C | Peak temp °C | Time above 217°C | Max. falling slope °C/s |
|-----------------|------------------------|--------------------|---------------------|--------------|------------------|-------------------------|
| Under Component | 3.0                    | 145 to 160 sec     | 50 to 65 sec        | 241 to 244   | 45 to 65 sec     | -2 to -3                |

### Post-Assembly Inspection

The post assembly inspection consisted of a continuity verification using an ohmmeter, a visual inspection to identify any popcorning or PWB damage, and x-ray to document voiding and verify solder ball alignment. One component from each test group was removed from the test board after assembly for use as a baseline comparison to thermally cycled solder joints.

### Thermal Cycling

Each test board was attached to an event detector with a threshold trigger set to 300 ohms for 200ms and then subjected to thermal shock cycles from -40°C to 125°C. The cycle combined 14-minute dwells at temperature extremities with 4-minute transition periods with a total of 36 minutes per cycle. The chamber set points were set above and below the respective hot and cold temperature targets for short durations at the beginning of each soak and then changed to the target temperature of -40°C or 125°C. The effect was to maximize the time of the boards at the soak temperatures. Time at temperature during the hot and cold soak was approximately 9.5 minutes at hot and 11 minutes at cold. Measurements began when the board temperature was within 5 degrees of the set point. Tests were to be conducted in a single chamber.

Components were removed from test as soon as possible after a failure was recorded. After 2000 cycles, components showing no failure were also removed for comparison to the failed components. Testing was terminated at 6500 cycles and additional non-failed components were sectioned, to offer a comparison to the failed components.

### Failure Analysis

Components with failed solder joints were x-rayed and then cross sectioned for evaluation. Information was gathered on the intermetallic growth in the solder joints, crack propagation and the effects of voids in the solder joint on the crack propagation using x-ray, a metallurgical and scanning electron microscope (SEM).

Most samples were not etched. Those that were etched were processed using a solution of HCl and methanol.

## Results and Discussions

### Post Assembly Inspection

Two opens were found after assembly. In the first case, a single Sn/Ag solder ball was scavenged into a neighboring solder ball on one component. No attempt was made to identify the cause. In the second open, a small piece of polyimide tape remaining on the bottom of a Sn/Ag/Cu solder ball, prevented contact between the solder ball and the solder paste. A bridge was formed in the daisy chain to by-pass the opens to enable testing.

### Visual

Rough surfaces typical of Pb-free solders were observed in the stereomicroscope. Nothing unusual was seen in the size shape or registration of the solder balls on the PWB.

### X-Ray

Component registration to the solder pads was consistent on all assembled samples. Solder joints with all three alloys were mostly void free. Voids that did occur most often constituted less than 2% or smaller of the cross sectional area of the solder joint as measured with x-ray.

A discernable increase in voiding was observed in Pb-free solders as compared to the Sn62 solder.

#### **Cross Sectional Analysis –Voiding, As Assembled**

Ni/Au surface finish produced numerous small voids found in and around the intermetallic formations at the solder interface. These small voids were more numerous in the SAC, and Sn/Ag solders as compared to the Sn62 solder. They were so small that they were not identified in the xray inspection. Examples of the small voids are shown in Figures 1 and 2. Small voids were rare at the interface of Cu/OSP solder pads.

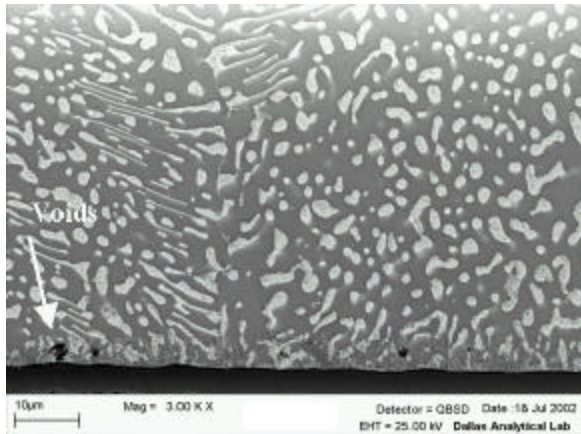


**Figure 1 - Eutectic Sn/Pb Solder Joint on ENIG after Assembly Small Voids at Interface were Typical of all Ni/Au Solder Joints**

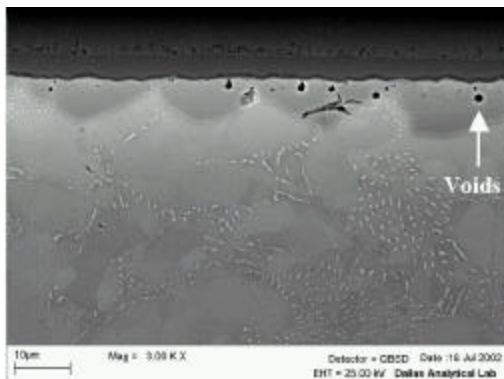


**Figure 2 - Sn/Ag Solder Interface to ENIG on Component Side**

#### **Cross Sectional Analysis–Intermetallic Compounds**

The ENIG to solder interface of both the components and the PWBs contained a layer of high phosphorous content Ni and cracking that are typical of black pad defects.<sup>9-12</sup> Au introduced from the board and component surface finishes was thoroughly dispersed in all the solder joints and constituted such a small weight percent of the solder that it was not identifiable by EDS analysis. There were however, other significant differences in the intermetallic formations in the solder joints from each alloy and surface finish combination.

The composite intermetallic thickness for the various lead-free BGA solder alloys were examined and compared with values and composition identified in literature.<sup>6, 13-18</sup> EDS analysis was used to identify commonality of IMCs with these published reports and not to determine precise elemental measurements. The presence of large plate, needle and rod intermetallic structures near the pad interface have been excluded from the average thickness measurements to allow comparison of the formation of the continuous or near continuous layers of Cu-Sn or Ni-Sn near the pads. For the Ni pads, the measured thickness is primarily for the Ni<sub>3</sub>Sn<sub>4</sub> layer. The Cu-Sn intermetallic layers in general form at much thicker levels compared to assemblies aged on Ni pads. The lead-free solders also show larger as assembled intermetallic thickness levels.

#### **SnPb + Sn62 IMC**

IMCs in solder joints with ENIG on both the component and the PWB were primarily Ni<sub>3</sub>Sn with small amounts of a (Ni)P compound detected<sup>19</sup> but was not thoroughly investigated. After temperature cycling, a continuous layer of Ni<sub>3</sub>Sn<sub>4</sub> formed between the phosphorous rich layer of Ni and the crystals and needle like formations of the Ni<sub>3</sub>Sn.<sup>20</sup>

The eutectic control solder joints consisted of a uniform distribution of Sn and Pb with small grains. Grain boundaries contained very small amounts of small spheroidal particles of Ag<sub>3</sub>Sn. Interfacial areas contained the expected intermetallic compounds of Cu<sub>6</sub>Sn<sub>5</sub> and Cu<sub>3</sub>Sn on the copper OSP solder pads. Cu available from the OSP pads did migrate to the component formed (Ni,Cu)<sub>3</sub>Sn at the interface with ENIG solder pads on the components. Small amounts of Cu<sub>6</sub>Sn<sub>5</sub> needles were also found in the bulk solder.

#### **Sn/3.5Ag IMC**

Figure 2 shows an example of the intermetallic compounds formed in SnAg solder at the ENIG interfaces on an ENIG finished PWB. IMCs in solder joints with ENIG on both the component and the PWB were primarily Ni<sub>3</sub>Sn with small amounts of Ni<sub>3</sub>P. The maximum height of the IMC peaks was approximately 6µm. A continuous layer of Ni<sub>3</sub>Sn<sub>4</sub> formed between the phosphorous rich Ni layer after thermal cycling. The IMC formations from SnAg on OSP finished PWBs were different at the PWB and component interfaces. After assembly the IMCs at the PWB interface consisted mainly of Cu<sub>6</sub>Sn<sub>5</sub> as shown in Figure 3. The SnAg/OSP combination produced the thickest IMC formation at the solder interface when compared with the other samples. It measured up to

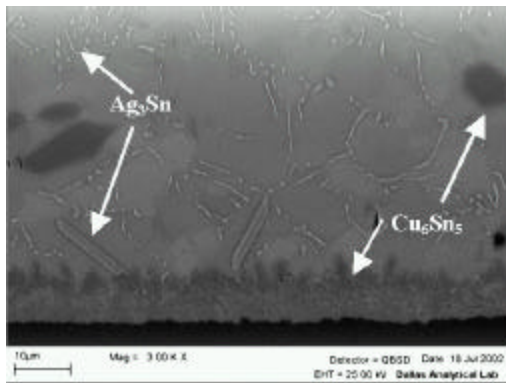


**Figure 3 - Sn/Ag Solder at Cu/OSP Interface after Assembly  $Ag_3Sn$  Forms in the Grain Boundaries Hexagonal  $Cu_6Sn_5$  is seen in the Bulk Solder**

9µm in thickness but was more commonly near 5µm. These measurements were consistent with samples assembled by other consortium members.<sup>8, 21</sup> The IMC on the component side of an OSP PWB remained similar to the structure seen in Figure 2, but with the addition of  $Cu_6Sn_5$  and,  $(Ni,Cu)_6Sn_5$  needles above the  $Ni_3Sn$ .

Small plates, spheroids, and elongated particles of  $Ag_3Sn$  formed mostly in the small angle grain boundaries of the solder. The small plates are more clearly seen in an etched sample shown in Figure 4. Large plates of  $Ag_3Sn$  were occasionally found at random locations and orientations in the bulk solder. These larger plates were more common in the SnAg/OSP components. EDS analysis identified a small percentage of Cu in the plates but this was not fully investigated at the time of this report. The population of large  $Cu_6Sn_5$  needles was similar to that of the Sn62/OSP solder joints but with a slight increase.

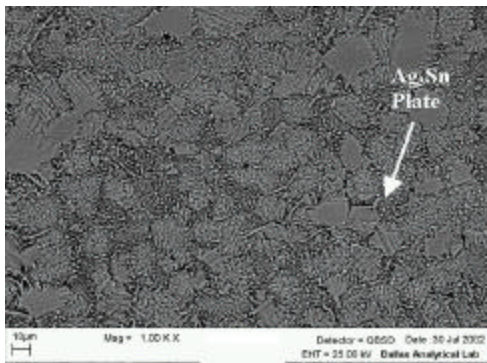


**Figure 4 - Typical Morphology of Sn/Ag Solder Joints with Small Grain Size and Numerous  $Ag_3Sn$  Plates in the Grain Boundaries - Etched Sample**

#### ***Sn/3.8Ag/0.7Cu IMC***

The IMC compounds formed with the ENIG/SAC combination were similar to those observed with the SnAg solder. However, the  $(Ni,Cu)/Sn$  IMC compounds at the interface with ENIG changed from a block-like structure seen in Figure 2 to a needle-like structure seen in Figures 5 and 6. The layer was also thinner with an average near 4µm. The layer consisted of  $(Ni,Cu)_6Sn_5$ ,

$(Ni, Cu)_3Sn$  and a layer of  $Ni_3Sn$  that increased in thickness as thermal cycling progressed. Large  $Ag_3Sn$  plates and voids similar to those shown in Figure 7 were more numerous when compared to the SnAg solder.

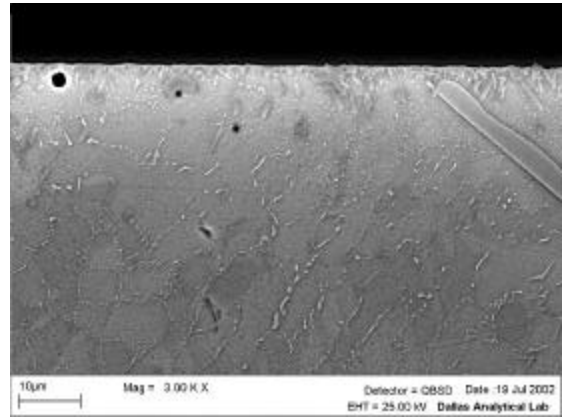


**Figure 5 - Intermetallic Formations Seen at ENIG/SAC Interfaces**

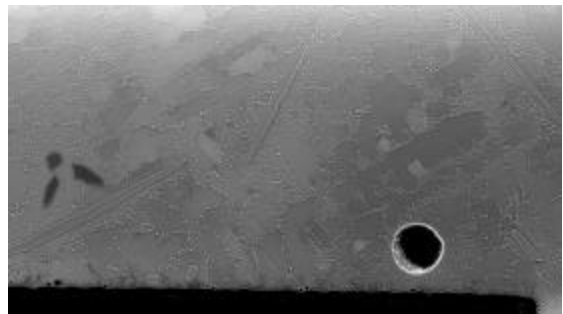


**Figure 6 - Typical SAC on Ni/Au Bulk Solder at 1000x.  $Cu_6Sn_5$  is Seen at Left above an  $Ag_3Sn$  Plate**

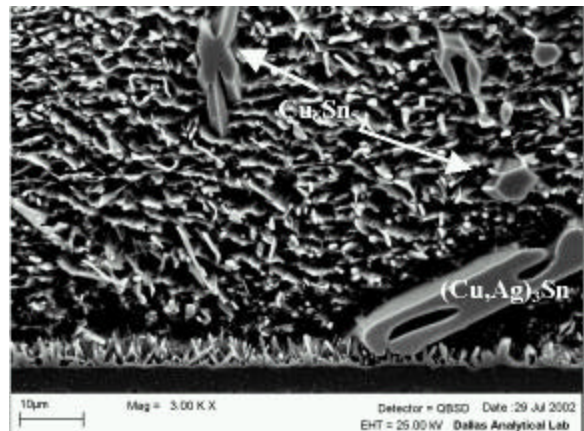


**Figure 7 - Etched Sample of SAC Solder on OSP after Assembly**

With the OSP/SAC combination, the IMC thickness averaged near 5µm or nearly half the maximum thickness found on the SnAg/OSP combination. A representative sample of the interface is shown in Figure 7 after extended etching. An  $Ag_3Sn$  plate is seen in the lower right hand corner and hexagonal end  $Cu_6Sn_5$  needles can also be seen.  $Ag_3Sn$  plates  $Cu_6Sn_5$  needles were randomly dispersed and oriented in the solder balls. The star shaped

structure at the top of the image is also  $\text{Cu}_6\text{Sn}_5$  and is a result of the increased Cu content of the solder joints. It is similar to the Cu-Sn structure found in Babbitt, which has a Cu content of 7%.<sup>22</sup> Figure 8 shows the star structure with greater clarity. EDS measured the Cu content in the bulk solder joint at approximately 6 wt%.

The void in Figure 8 is representative of many truncated voids seen during this investigation. They were often attached to an  $\text{Ag}_3\text{Sn}$  plate. It is hypothesized that the plates interfere with the evolution of voids during the soldering process.

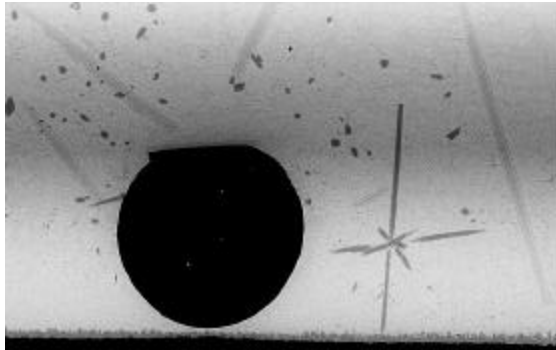


**Figure 8 - SAC on OSP at 1000x. Cu Intermetallic Formations are Found in the Bulk Solder Including the  $\text{Cu}_6\text{Sn}_5$  Star -  $\text{Ag}_3\text{Sn}$  Plates are most Common in this Metallurg**

The spheroidal, elongated and plate-like structures of  $\text{Ag}_3\text{Sn}$  were found in small angle grain boundaries throughout the bulk solder.<sup>23-24</sup> Figure 9 shows a heavily etched SAC solder ball. The spheroidal  $\text{Ag}_3\text{Sn}$  particles can be seen where they form in the grain boundaries between Sn rich areas. It was observed that the particles increase in size with closer proximity to the Ag/Sn plates. These larger elongated particles contain 3-5 weight percent Cu and the Ag/Sn plates contain up to 7% Cu as measured by EDS. This identified Cu as a key component for the formation of the larger particles and plates that are more correctly labeled as a  $(\text{Cu},\text{Ag})_3\text{Sn}$  compound.

Figure 10 provides a perspective on the size, location, and distribution of the  $\text{Ag}_3\text{Sn}$  plates within SAC solder balls on OSP. The solder balls have been through 6500 thermal cycles without failure. An extended etch was used to highlight the plate formation. Evaluation of adjacent solder balls shows the variations in plate formation from one solder ball to another on the same component. The solder ball on the left is at the corner of the component.

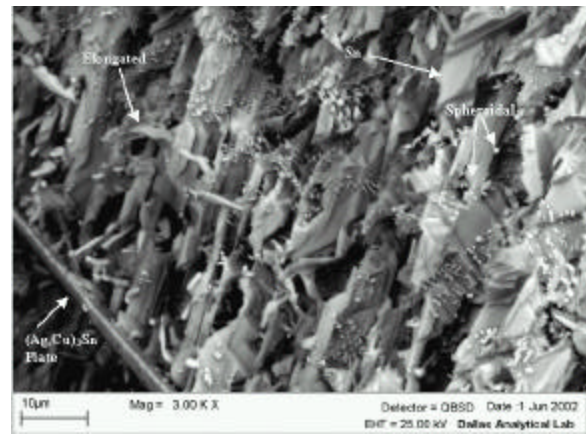


**Figure 9 - Etched Sample of SAC/OSP showing  $\text{Ag}_3\text{Sn}$  - Spheroidal, Elongated, and Plate in Sn Matrix**

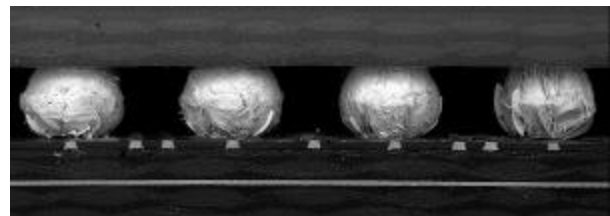


**Figure 10 - Extended etch of SAC/OSP Solder Joints show the Range of Variations in IMC Content in Adjacent Solder Joints**

A magnified view of the right hand solder ball is shown in Figure 11 and is presented as an extreme example as the number and size of intermetallic formation in this joint was not common for solder balls in this study. The two  $(\text{Ag},\text{Cu})_3\text{Sn}$  plates on the left extended from the top to the bottom of the solder joint before being broken after etching.  $(\text{Ag},\text{Cu})_3\text{Sn}$  plates could be found throughout the solder joints, but were generally observed more often toward the PWB side of the joint.

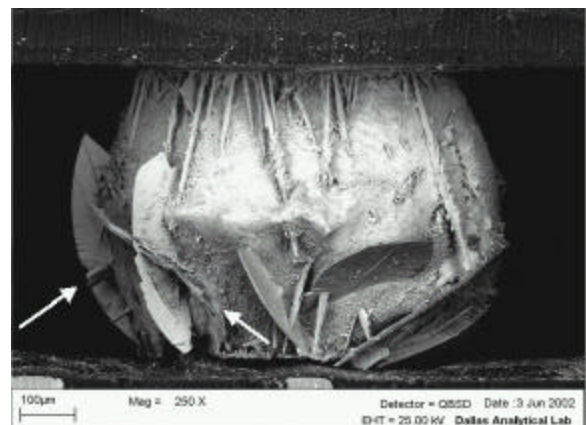


**Figure 11 - Magnification of Solder Ball in Figure 10 shows Maximum IMC Content that was Found - Plates are  $(\text{Ag},\text{Cu})_3\text{Sn}$  and Needles are  $\text{Cu}_6\text{Sn}_5$**

$\text{Cu}_6\text{Sn}_5$  needles extend from both interfaces toward the middle of the solder joint. The long needle on the right shows the extent of needle length. Adjacent solder balls in

Figure 10 did not have needles of this length.  $\text{Cu}_6\text{Sn}_5$  needles can also occur in a transverse direction and are also seen intersecting the  $(\text{Ag,Cu})_3\text{Sn}$  plates in several locations two of which are indicated by arrows.

**Whisker Growth**

Cross sectional analysis of the Pb-free solder joints revealed Sn whiskers growing within some voids. Figure 12 shows Sn whiskers extending from the surface of an internal void in a Sn/Ag solder joint on an ENIG PWB after 2700 temperature cycles. Similar whiskers were also found in SAC solder joint voids at various stages of thermal cycling.

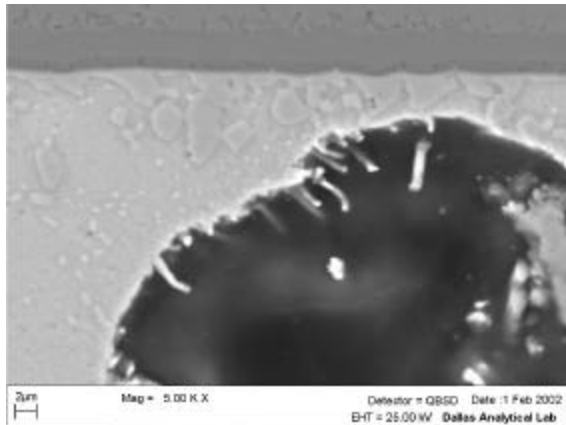


**Figure 12 - Sn Whiskers found on the Surface of Internal Voids in Sn/Ag and SAC Solder Joints**

Figure 13 shows a magnified view of the whiskers. The size and shape of the whiskers are non-uniform with the body conforming somewhat to the shape of the Ag compound found at the end of each whisker. The Ag compound on the end is similar in size and shape to the small  $\text{Ag}_3\text{Sn}$  particles found throughout the bulk solder. Proposed theories about the formation of Sn whiskers suggest a compressive force is acting on the voids.<sup>25</sup> It demonstrates the potential for whisker growth in these high Sn solders.

Optical and x-ray inspection after test termination at 6500 cycles, located growths or protrusions on the side of many of the Sn/Ag and SAC solder joints.

Figure 14 shows an xray image of the largest of the protrusions as seen from the top of the component and Figure 15 provides a side view of these same solder balls. All the other protrusions found on Sn/Ag and SAC were needle like in shape. However, in this case, the protrusions are large Sn rich formations growing out from regions between two vertical cracks in the solder balls. These vertical cracks will be discussed further in the Failure Mechanisms section. Please note the neighboring solder balls are free from horizontal or vertical cracking. The sample was SAC/ENIG and had completed 6500 thermal cycles without a recorded failure. The dark horizontal line on the solder balls is flux residue.

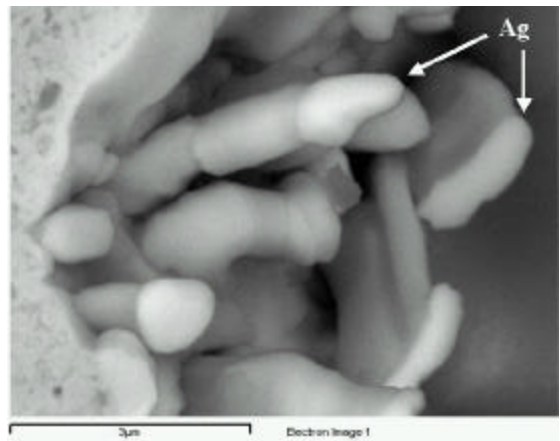


**Figure 13 - A Magnified View of Sn Whiskers Inside a Solder Void - Lighter Colored End of the Whisker is an Ag Compound**

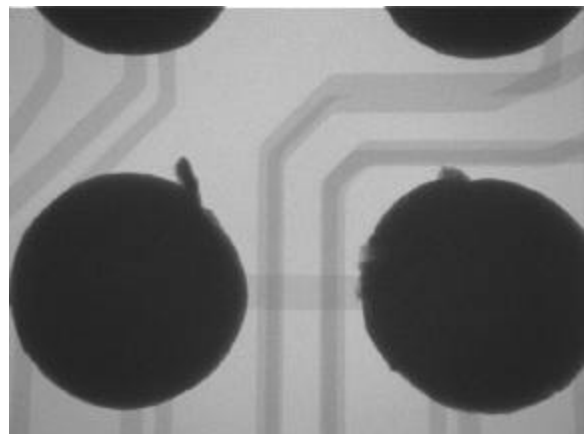


**Figure 14 - This x-ray Image shows Sn Growths at the Edge of Two Solder Balls**

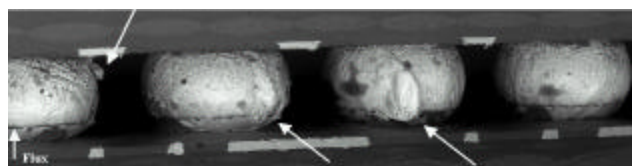


**Figure 15 - 75x Image of Sn Rich Protrusions on SAC/OSP Solder Balls after 6500 Cycles (See Figure 28)**

**Failure Mechanisms and Reliability**

The earliest failure occurred with the combination of ENIG surface finish and SAC solder after 12 thermal cycles. Intermetallic compounds were formed but a clean separation occurred across the entire solder joint at the interface between the solder and the Ni. The phosphorous rich layer was seen as a dark band at the outer surface of the Ni layer and was found on all ENIG plated surfaces in this study. Five additional SAC/ENIG components had the same failure mechanism from approximately 180 to 400 temperature cycles. Four of these six early failures occurred at the component interface.

Similar failures occurred with 5 SnAg/ENIG solder components between 180 and 1051 temperature cycles. The difference in the failures is shown in Figure 16 where only a partial separation occurred at the Ni to solder interface. Up to one half of the fracture was in the bulk solder above the intermetallic compound formations. The continuous Ni<sub>3</sub>Sn layer can be seen at the surface of the phosphorous rich Ni layer in Figure 16. These were not deemed to be solder fatigue failures.

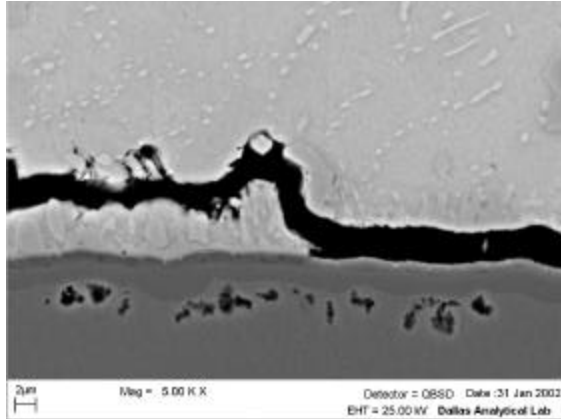


**Figure 16 - PWB Side Failure at 650 Cycles on SA/ENIG Construction**

Component delamination was initially seen in samples taken at 2000 cycles. Separation typically started at the edges of the glass slide and could be seen with a simple visual inspection. The delamination of the glass was not extensive at this point however, Figure 17 shows cracks progressing from under the glass slide, through the underfill material, and into the component substrate laminate at 2000 cycles. It is suspected that the delaminations did influence the CTE mismatch between the component and the PWB and resulted in some out of plane stresses. Figure 17 also shows the relative position of the edge of the glass plate to the corner solder balls.<sup>8</sup> The deformation and grain coarsening of PbSn solder shown in Figure 18 indicate the areas of greatest stress on the solder joints.

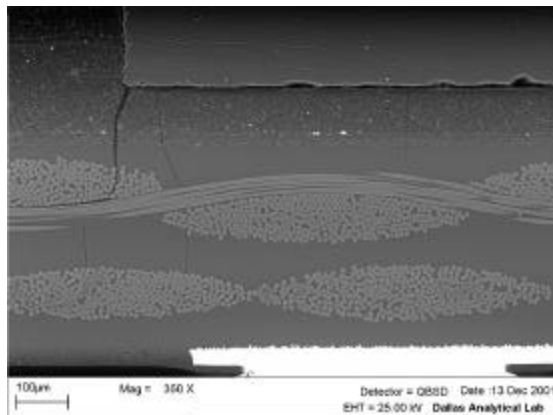


**Figure 17 - Delamination in the Component as Seen after 2000 Temperature Cycles**

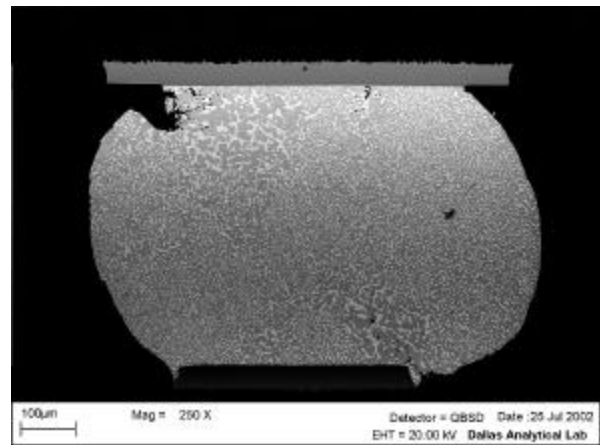


**Figure 18 - Representative Grain Coarsening and Deformation of Eutectic Sn/Pb Solder Joint after 6500 Cycles**

Delamination of the glass slides continued to progress with additional thermal cycling. It was decided to terminate the temperature cycling at 6500 cycles owing to evidence of delamination that was seen on most of the remaining components. Total failures at the end of testing are listed in Table 2. Totals reflect the removal of some components for analysis before failure.

**Table 2 - Total Failures after 6500 Cycles**

| Solder/Surface Finish | SnPb/Sn62 | SnAg  | SAC   |
|-----------------------|-----------|-------|-------|
| ENIG                  | 12/15     | 26/30 | 12/30 |
| OSP                   | 14/15     | 15/30 | 12/30 |

X-ray inspection gave indications of the formation of vertical cracks in components as early as 2700 cycles. The solder balls with the vertical cracks were located randomly across the arrays of the Pb-free components with surrounding solder balls being unaffected as shown in Figure 19. There were no vertical cracks found in the Sn/Pb solder joints.

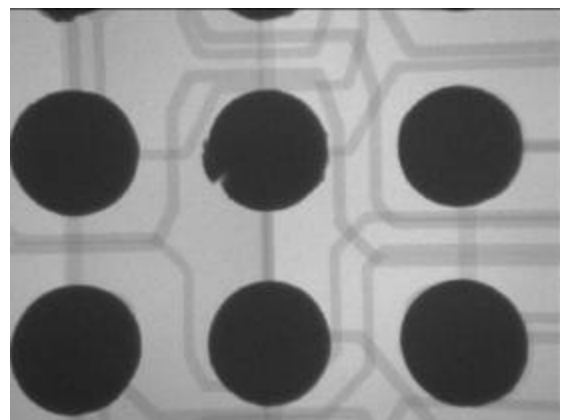


**Figure 19 - X-ray Image showing a Vertical Crack in a Sn/Ag Solder Joint after 6500 Temperature Cycles**

Cross sectional analysis and inspection of the exterior surfaces of the solder balls revealed several unique failure features in Pb-free solder joints. They include crack propagation along multiple fronts, crack propagation paths being altered by  $\text{Ag}_3\text{Sn}$  plates, vertical and horizontal fracture, shrinkage voids or sinkholes, and the potential of spalling of portions of the solder joints. In addition, large angle grain boundaries were found to be among the preferred paths for crack propagation.

Multiple fractures occurred in the small angle grain boundaries in the Sn rich solder matrix giving a shattered look to the failures as seen in Figure 20. Cracks often progressed away from the solder interface or secondary cracking occurred (Figure 20). The frequency of fractures occurring on the component side and the PWB side of the solder joint was approximately equal.

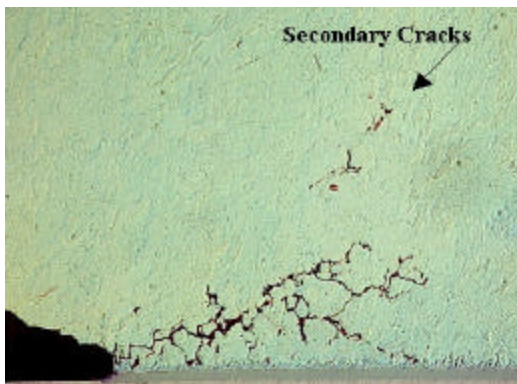


**Figure 20 - Multiple Cracks Propagate through Small Angle Grain Boundaries in Pb-Free Solder**

Figure 21 shows a SAC solder joint after 2700 cycles where crack propagation has been modified by the presence of the  $(\text{Ag,Cu})_3\text{Sn}$  plate. In an electrically “good” solder ball after 6500 cycles, the crack propagation at the pad interface in Figure 22, appears to have been arrested or retarded by the presence of the  $(\text{Ag,Cu})_3\text{Sn}$  plate. At the same time, the intermetallic plate at the right edge of the solder ball likely contributed to the initiation of vertical cracks at each end of the plate.

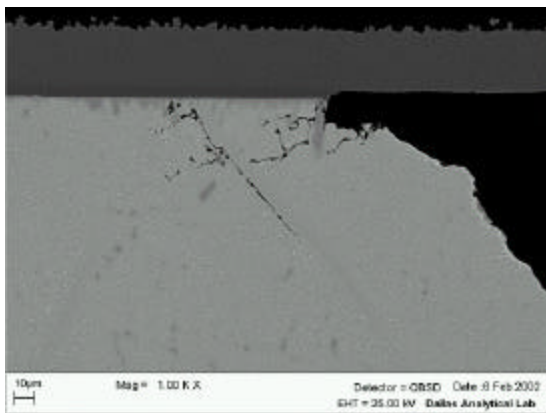


**Figure 21 - Fracture Path is Modified by the Presence of an  $\text{Ag}_3\text{Sn}$  Intermetallic Plate (2700 Cycles, SAC)**

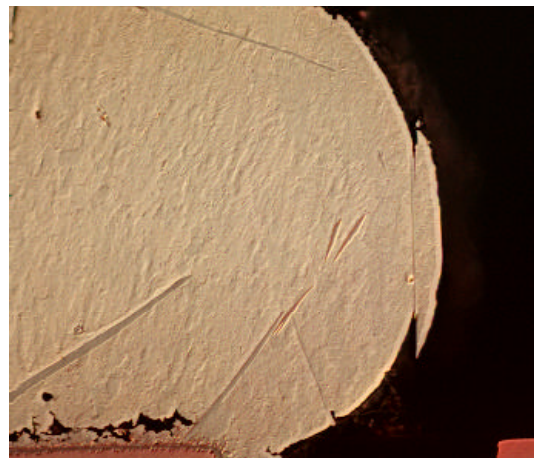


**Figure 22 - Intermetallic Plates can Retard Crack Growth or Influence the Crack Initiation (SAC/ENIG, 6500 Cycles)**

The inspection of the exterior of the solder balls provides an improved view of the vertical cracks seen in the x-ray. Figure 23 shows a vertical crack on the outside of a Pb-free solder joint. The magnification shows Sn plates fanning out perpendicular to the crack on the left side and parallel the crack on the right side indicating continuing modification of the solder structure. The cracked material at the base of the solder joint and the dark areas on the side of the solder ball are flux.

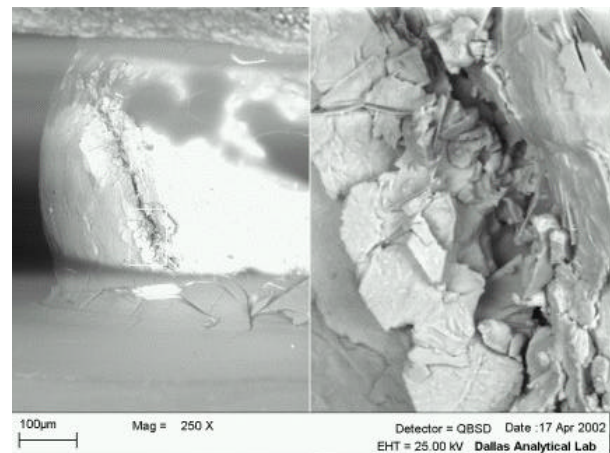


**Figure 23 - A Vertical Crack in a Sn/Ag on Ni/Au Solder Joint after 6500 Cycles**

Horizontal cracks were also found along the center plane of several solder balls as shown in Figure 24. The cracks on the outside of the solder balls were often accompanied by an increased surface coarseness and by “shrinkage voids” or “sink holes”. These terms attempt to describe the appearance of the solder that may have melted away at the locations leaving a hole surrounded by needle-like formations and spherical nodes with smooth surfaces. The phenomenon has been reported previously.<sup>26</sup> More often than not, no fracture surfaces were found in and around the shrinkage voids. It is possible that these features were initiated as cracks and the fracture surface was modified

over time in thermal cycling. An example of the typical surface roughness and needle like formations surrounding a sinkhole is shown in Figure 25.

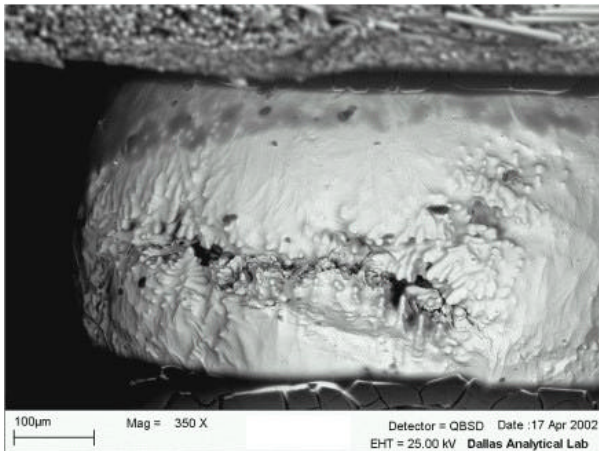


**Figure 24 - A horizontal Crack in a Sn/Ag Solder Joint after 6500 Cycles**

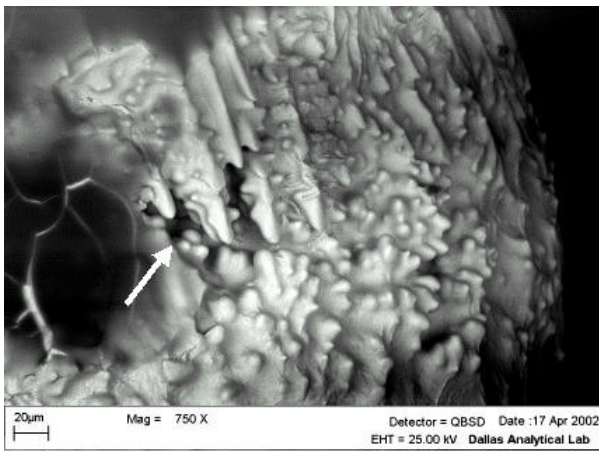


**Figure 25 - Typical Surface Roughness on Sn/Ag after 6500 Cycles - Arrow indicates the Location of a “Sink Hole”**

Cross sections of the sinkholes showed no fractured surfaces; rather the surfaces are populated with the rounded shapes of Sn dendrites. Figure 26 shows in cross section that the sinkholes can progress to a significant depth in the solder joint. Three sinkholes of ranging from approximately 25µm to 150µm are shown in a SAC/ENIG solder joint after 6500 cycles. The spherical or rounded structure of the Sn near the sinkholes is shown in Figure 27.

Shrinkage voids were found in SAC solder joints after assembly but they did not extend as deeply into the solder joints, the nodular surface was not well defined, and the needles shown in Figure 25 were not seen. No investigation was conducted to determine possible growth of the shrinkage voids present after SAC assembly. Shrinkage voids were not found in SnAg or SnPb solder after assembly but sink holes were present in all tested

combinations of the SnAg and SAC Pb-free solders when the joints were examined after 6500 cycles.

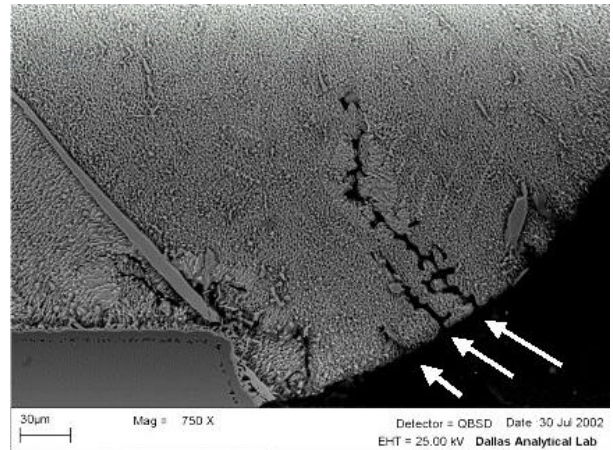


**Figure 26 - “Sink Holes” in a SAC on ENIG after 6500 Cycles - Solder Surface is Etched**

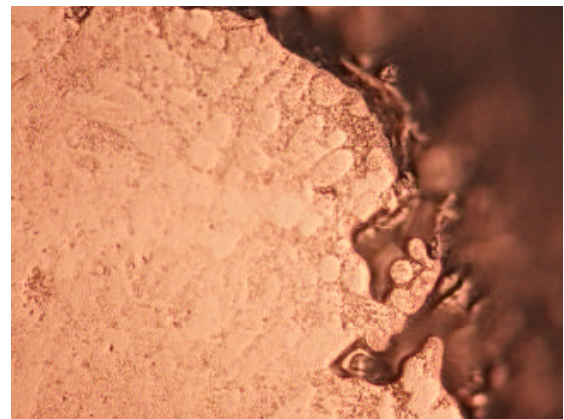


**Figure 27 - The Metallographic Image of an Etched Sn/Ag Solder Joint at 500x shows the Spherical Structure of the Sn in and Around the Sinkholes**

Flux residue was removed and the samples were etched in a solution of HCl and methanol to highlight the solder joint structure corresponding to the location and orientation of the cracks and sinkholes. After etching the exterior of both SnAg and SAC solder balls, it was readily apparent that the fracture locations and the sink holes were often associated with large angle grain boundaries in the solder joints. For example, the left center solder ball in Figure 15 is shown in Figure 28 after etching. Arrows indicate the protrusion growing from the solder ball at one large angle grain boundary and sink holes in the central grain boundary. The exterior views however, give little indication as to the contribution of intermetallic plates to the location of the cracks. Cross sections were examined to try and determine if the  $(Ag,Cu)_3Sn$  plates provided stress concentrations that led to the horizontal and vertical cracks. Findings indicate that the large angle grain boundaries are the preferred path for crack propagation with or without the intermetallic plates.

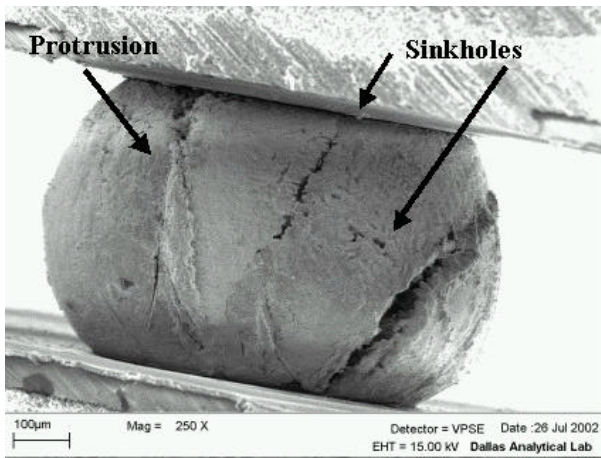


**Figure 28 - Vertical Cracks and Sinkholes in SAC/OSP Solder Ball - shown after Etch (See Figure 16)**

Figure 29 shows a representative sample of the variations that can occur in grain boundary orientation and location in adjacent solder joints. An enlargement of the center joint is shown in Figure 30. Numerous Sn/Ag and Sn/Cu intermetallic formations and their position in relation to the large angle grain boundaries are shown in the cross section. The solder joint has been through 6500 temperature cycles. A crack was initiated near the outside edge of a (Ag,Cu)<sub>3</sub>Sn plate near the upper left. Although the intermetallic plate runs almost parallel to the solder pad, the crack did not propagate along the intermetallic plate. Instead, the main damage to the joint occurred vertically in proximity to a large angle grain boundary and a (Ag,Cu)<sub>3</sub>Sn plate. Many larger intermetallic formations are found to some extent in the large angle grain boundaries but they do not precisely follow the boundary. Others transcended several large angle boundaries and sometimes lie perpendicular to the boundaries while others lie wholly within the grain colony.

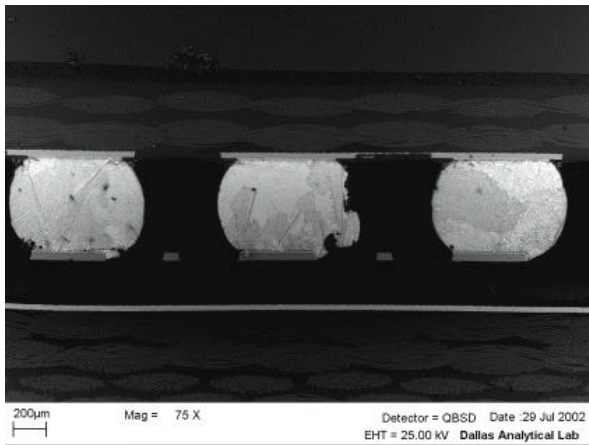


**Figure 29 - SAC Solder Joints after Etching show Variations in the Locations of Large Angle Grain Boundaries after 6500 Temperature Cycles**



**Figure 30 - Magnification of the Center Solder Joint**

The findings show that the main factor in producing the horizontal and vertical cracks is the large angle grain boundaries. Sn/Ag solder joints produced very few large Ag<sub>3</sub>Sn plates yet horizontal and vertical cracks formed in the bulk solder of many of those joints as well. Crack propagation can be seen at several locations in Figure 31 corresponding to large angle grain boundaries without large intermetallic plates. This solder joint failed at the component after 1138 cycles.

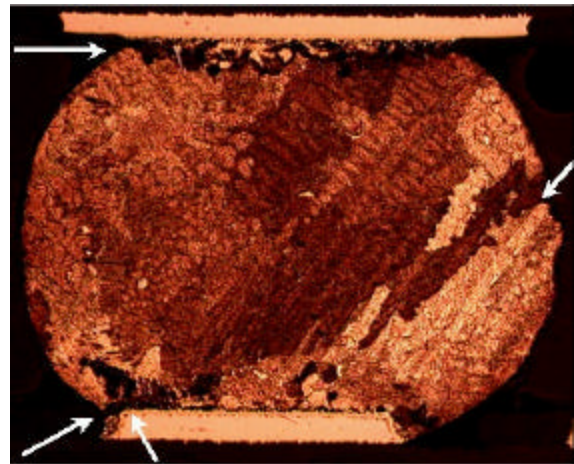


**Figure 31 - Metallographic Image of a Sn/Ag on Ni/Au Solder Joint after 1138 Cycles - Arrows Indicate Crack Locations and Direction of Progress**

A crack extending through the bulk solder near the component interface drops into the solder following large angle grain boundaries. Cracks have also initiated at large angle grain boundaries indicated by the arrows at the base and middle of the solder joint. Cracks run roughly parallel to the direction of the arrows along the grain boundaries. No large intermetallic plates were found in this cross section.

The (Ag,Cu)<sub>3</sub>Sn plate at the base of the joint in Figure 32 shows how the intermetallic plates often cross the large angle grain boundaries. Sinkholes can also be located away from the large angle grain boundaries.

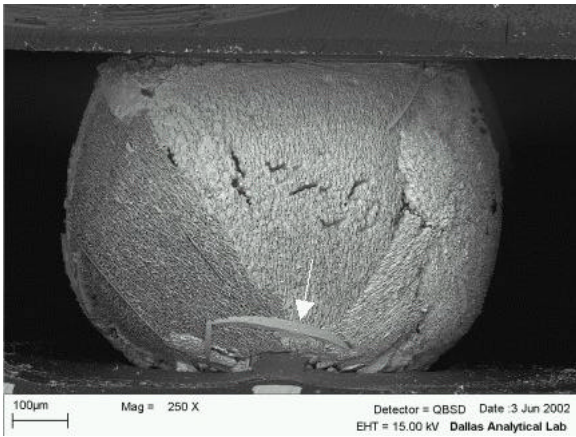


**Figure 32 - A (Ag,Cu)<sub>3</sub>Sn Plate Transcends Large Angle Grain Boundaries on the Outside of a SAC/ENIG Solder Joint after Etching**

Spalling of portions of the solder joint may be a problem for applications with long life requirements. Figure 33 shows a SAC solder joint that appears to be missing a portion of the original solder ball after 6500 cycles. Although a (Ag,Cu)<sub>3</sub>Sn plate is located near the fracture, the crack did not propagate along its surface. Solder missing in this and other joints led to additional x-ray inspections to locate solder that spalled off the solder balls and inspection of the exterior of the solder balls. No spalled pieces of the solder joints were found using x-ray analysis. However the boards were tested, stacked, and transported on edge and spalled portions of solder could have fallen out through normal handling. It was not determined if the missing portion actually spalled off or if the plane of the sections corresponds to the location of vertical cracks. Further studies will need to be done to verify the risk of spalling.

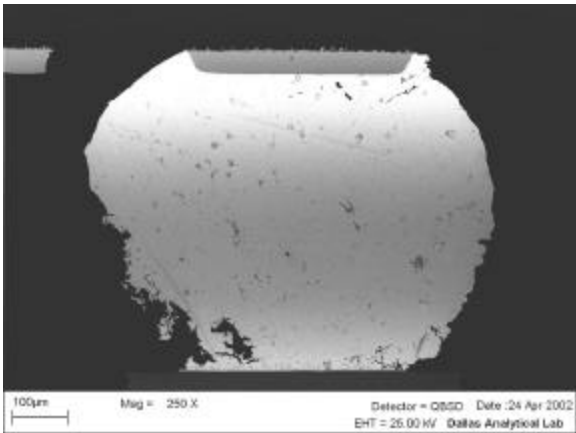


**Figure 33 - This Cross Section may Indicate the Potential for Spalling of Sections of Solder from the Joint (SAC/OSP, 6500 Cycles)**

### Reliability

In temperature cycling from -40°C to 125°C the SAC solders generally provided the best reliability. Tests conducted by other consortium members provided contrasting results when cycling from 0°C to 100°C.<sup>8</sup>

Variations in reliability can be attributed to differences in reflow profiles and cooling rates. In -40°C to 125°C conditions, SAC solder joints, which can have a significant number of large intermetallic formations, demonstrated higher reliability than the Sn/Ag solder joints containing mostly small plates in the small angle grain boundaries. Reliability plots are available in the companion paper.<sup>8</sup>

The location of the failures did not follow the distance to the neutral point (DNP) model. While some corner joints failed first, failures were just as likely to occur on any solder joint located on an interior row. Details of die penetrant testing that further describes the failure locations is given in the companion paper.<sup>8</sup>

### Conclusions

The conclusions reached through this study are as follows:

- SAC on OSP shows equivalent or better performance than eutectic Sn/Pb and Sn3.5Ag solders in temperature cycling tests from -40°C to 125°C.
- Ultimately, fatigue failures in the Pb-free solders were in the bulk solder above the PWB and component interfaces not the IMC layer. This is an important finding since the increased Pb-free processing temperatures produced increased intermetallic formation at the interfaces.
- Intermetallic compounds can be beneficial to SAC reliability. (Ag,Cu)<sub>3</sub>Sn intermetallic plates can arrest or redirect crack propagation when oriented transverse to the large angle grain boundaries in the solder.
- Crack propagation in Pb-free solders can proceed preferentially along large angle grain boundaries in the solder joints. Vertical and horizontal cracks can occur at any location in solder joint. Their location in a solder ball array as well as their orientation and location on a solder joint are as random and unpredictable as the locations of the large angle grain boundaries.
- Predicting the reliability of area array components based on neutral point calculations may be more complicated. Current solder fatigue reliability models do not account for preferential crack propagation in the large angle grain boundaries of the solder joints.
- There is still potential for Sn whisker growth. High Sn content protrusions found in this study indicate the risk is not limited to whiskers.
- Spalling of portions of the solder joints is possible in high cycle applications owing to the significant damage to solder joints along the horizontal and vertical large angle grain boundaries. This damage occurs long before ultimate failure.
- Voids can attach to IMCs slowing the evolution of gases and may be a possible factor in void retention in Pb-free systems.

Pb-free processing is viable for many applications. Improved reliability of SAC solder over eutectic SnPb solder has been demonstrated. But there is much we do not understand. This study shows that any new application of Pb-free solders with extended lifetime requirements must be evaluated on an individual basis to ensure suitability for those application specific requirements.

### Acknowledgements

The authors would like to thank the Universal Instruments Consortium for providing the components and PWBs for testing, and the opportunity to participate in the study. At Nokia, Marshall Turman, Carlos Wilson, Frank White, and JoAnn Turpin provided support for the assembly. Puligandla Viswanadham (Nokia Research), Sridhar Canumalla (Nokia, Dallas Analytical Lab) and Paul Vianco (Sandia National Labs) are acknowledged for their valuable discussions and review of the text. Robert Champaign and Marlin Downey from the Raytheon failure analysis laboratory also provided exceptional support. Thanks also to the Nokia management team for supporting our participation in this collaborative research with Universal Instruments Consortium and its members.

### References

1. T. Laine-Ylijoki, Dr. H. Steen, A. Forsten, "Development and Validation of a Lead-Free Alloy for Solder Paste Applications," International Conference on Electronic Assembly: Material and Process Challenges, Atlanta, GA, May 29-31, 1996.
2. G.Grandi, J. Nykanen, T. Lepisto, " Intermetallic Compounds In Lead-free Soldering," Tampere University of Technology, Report #10, 1999.
3. W. Peng, K. Zeng, J. Kivilahti, "A Literature Review on Potential Lead-Free Solder Systems," Helsinki University of Technology, report series HUT-EPT-1 2000, ISBN 951-22-4979-0.
4. K. Zeng, W. Peng, J. Kivilahti, "Formation of Intermetallic Compounds in Solder Joints and Its Effects on Joint Reliability," Helsinki University of Technology, report series HUT-EPT-2 2000, ISBN 951-22-4980-4.
5. R. Kato, "Lead Free Solder for Environmental Protection", Sinju Metal Industry Co., Ltd., R&D Report, issued May, 1998.
6. S.K.Kang, et. al., "Interfacial Reaction Studies on Lead (Pb)-Free Solder Alloys," Proceedings 2001 ECTC, Lake Buena Vista, FL., May 29-June 1, 2001.
7. H. Danielsson, "Lead-Free Soldering Causes Reliability Risks for Systems With Harsh Environments," Advancing Microelectronics, May/June 2002, pp. 7-11.
8. M.Meilunas, A. Primavera, S.O.Dunford, "Reliability and Failure Analysis of Lead-Free Solder Joints," IPC 2002, New Orleans, LA, Nov 2-3, 2002
9. B.Houghton, "ITRI Project on Electroless Nickel/Immersion Gold Joint Cracking," IPC Printed Circuits Expo'99, March 14-18, 1999, Long Beach, CA, pp.S18-4-1 to S18-4-
10. N.Bunno, "A Root Cause Failure Mechanism for Solder Joint Integrity of Electroless Nickel/Immersion Gold Surface Finishes," Future Circuits International, 1998, pp. 133-137.
11. D.Goyal, et.al., "Failure Mechanism of Brittle Solder Joint Fracture In the Presence of Electroless Nickel Immersion Gold (ENIG) Interface," Proceedings of ECTC 2002, San Diego, CA., May 28-31, 2002.
12. R.F. Champaign, J.A.Roepsch, M.R. Downey, "Case Study: The Effect of Severe Black Pad Defect on Solder Bonds on Ball Grid Array Components", Proceedings, SMTA Advanced Technologies Symposium, Boston, MA, June 11-12, 2002, pp. 29 – 34.
13. Zribi, A., Zavalij, L., Cotts, E., Borgesen, P., Primavera, A., G. Westby, G. "Growth of Ternary Intermetallic Alloys in Pb-Sn and Cu-Ag-Sn Pb-free Electronic Joints" , Electronics Component and Technology Conference, 2001.
14. Bradley, E., and Banerji, K, "Effect of PCB Finish on the Reliability and Wettability of Ball Grid Array Packages", IEEE Transactions CPMT Part B, 1995, pp. 320-330.
15. Bradley, Edwin, Lall, P., and Banerji, K., "Effect of Thermal Aging on the Microstructure and Reliability of Ball Grid Array (BGA) Solder Joints", SMI Proceedings, Vol. 1, 1996, pp. 95-106.
16. S.K.Kang, et.al., "Interfacial Reactions, Microstructure and Mechanical Properties of Pb-Free Solder Joints in PBA Laminates," Proceedings of ECTC 2002, San Diego, CA., May 28-31, 2002.
17. Young-Doo Jeon, et al, "Studies on the Interfacial Reactions between Electroless Ni UBM and 95.5Sn-4.0Ag-0.5Cu Alloy," Proceedings of ECTC 2002, San Diego, CA., May 28-31, 2002.
18. P.Snugovsky, T.Siewert, C.McCowan, "Summary of Intermetallic Composition Studies For NEMI Lead-Free Reliability Task Force," For additional information see Interim Report.4.doc, and NEMI Report on Intermetallic Stoichiometry-final4.pdf in the Appendix.
19. K.Zeng, V.Vuorinen, J.K.Kivilahti, "Intermetallic Reactions Between Lead-free SnAgCu Solder and Ni(P)/Au Surface Finish on PWBs," Proceedings 2001 ECTC, Lake Buena Vista, FL., May 29-June 1, 2001.
20. K.Y.Lee, M.Li, D.R.Olsen, W.T.Chen, "Microstructure, Joint Strength and Failure Mechanism of Sn-Ag, Sn-Ag-Cu versus Sn-Pb-Ag Solders in BGA Packages," Proceedings 2001 ECTC, Lake Buena Vista, FL., May 29-June 1, 2001.
21. Universal Instruments Consortium Quarterly Meeting. June 4th-5th, 2002. Report Available from Mike Meilunas or Anthony Primavera.
22. S.H. Avner, "Introduction to Physical Metallurgy," McGraw Hill 1974, Second Edition, pp. 523, Fig. 12-41.

23. D.R. Frear, et al "Pb-Free Solders for Flip-chip Interconnects," JOM, 53(6)(2001), pp.28-32.
24. Y. Zheng, C. Hillman, P. McCluskey, "Intermetallic Growth on PWBs Soldered with Sn3.8Ag0.7Cu," Proceedings of ECTC 2002, San Diego, CA., May 28-31, 2002.
25. K.N.Tu, K.Zeng, "Reliability Issues of Pb-free Solder Joints in Electronic packaging Technology," Proceedings of ECTC 2002, San Diego, CA., May 28-31, 2002.
26. S.Dunford, P.Viswanadham, P.Rautila, "Metallurgical and Reliability Aspects of Lead-free Mixed Technology Electronic Assembly for Mobile Communication Products," IPC Works 2000, Sept. 9-14, 2000, Miami, FL.